J. Appl. Comput. Mech., 9(1) (2023) 83-94
DOI: 10.22055/jacm.2022.40666.3625

ISSN: 2383-4536
jacm.scu.ac.ir

Shahid Chamran University of Ahvaz

Journal of Applied and Computational Mechanics

Research Paper

Numerical Modeling of Fluid's Aeration: Analysis of the Power Losses and Lubricant Distribution in Gearboxes

Marco Nicola Mastrone[1], Franco Concli[2]

[1] Faculty of Science and Technology, Free University of Bolzano, Piazza Università 1, Bolzano (BZ), 39100, Italy, Email: mamastrone@unibz.it

[2] Faculty of Science and Technology, Free University of Bolzano, Piazza Università 1, Bolzano (BZ), 39100, Italy, Email: franco.concli@unibz.it

Received April 28 2022; Revised June 18 2022; Accepted for publication June 24 2022.
Corresponding author: M.N. Mastrone (mamastrone@unibz.it)

Abstract. Aeration determines the entrainment of air in another fluid. In geared transmissions, this process affects the operating temperature of the mechanical system because the air's bubbles trapped in the lubricant act as an insulator. Lubricant's aeration occurs mainly because the gears' teeth entering the oil sump and the oil impacting on free surface. Being able to numerically model aeration is fundamental to better describe the physics and the lubrication mechanisms which affect the behavior of the system. In this paper, a new solver that includes the aeration phenomenon was implemented in the opensource environment OpenFOAM®. The simulations' results were validated with torque measurements. Moreover, a comparison of the oil distribution between a standard multiphase- and the new aeration-solver is provided.

Keywords: CFD, aeration, power losses, lubrication, gearboxes.

1. Introduction

Nowadays, energy efficiency represents a fundamental aspect in mechanical design. Efficient solutions translate not only into pure energy saving, but also into a reduction of fuel consumptions, as in the automotive sector, and into higher systems' reliability due to lower operating temperatures. For this reason, the investigation on power dissipation in the first stages of the design phase is a key factor to optimize the load carrying capacity and the thermal conditions of geared transmissions. Higher power densities, design of more compact and lightweight solutions, and downsizing of mechanical systems are just some of the benefits of an accurate study on lubrication and power dissipation. To increase the efficiency of gearboxes it is important to implement adequate modelling techniques able to describe the physics of the problem accurately. In the recent years, a lot of effort was put in the development of new mesh handling strategies for the simulation of dynamic domains. One of the aspects where numerical models can be further developed is related to the interaction between multiple phases, except for immiscible fluids where numerical approaches as MULES (Multidimensional Universal Limiter with Explicit Solution) [1] and CICSAM (Compressive Interface Capturing Scheme for Arbitrary Meshes) [2] are commonly used. Complex multiphase problems involving various kinematics and dynamic systems have been numerically approached for the simulation of gearboxes. Lu et al. [3, 4] investigated the power losses of a helicopter gearbox including the thermal effects. Bianchini et al. [5, 6] simplified the geometry of a planetary gearbox by enlarging the gap between the teeth, thus avoiding the need of remeshing and exploiting the moving reference frame technique. As a result, the simulation time was reduced and information about the trend of the power dissipation could be gathered faster. Li et al. [7] compared different mesh motion strategies concluding that the use of dynamic mesh appears to be the best for flow and loss prediction, despite the higher computational costs with respect to other approaches. Liu et al. implemented virtual models for dip [8] and injection [9] lubrication, demonstrating the capability of the virtual models to capture the real physics observed experimentally. Recently, the authors have implemented an innovative remeshing procedure for the study of spur [10], helical [11] and bevel gears [12].

The increase in the computational power allowed to include in the calculations also additional physical phenomena as cavitation [13–17]. Pioneering studies on aeration in mechanical components can be found in [18, 19], where the authors analysed the aeration in tapered roller bearings with experimental and numerical investigations. The aeration phenomenon (interaction between a liquid and a gaseous phases of different fluids) has been poorly touched from a numerical point of view. This is mainly related to the fact that when aeration is low, it does not affect the power losses and the lubrication capability significantly. However, when the aeration level inside the transmission increases, the behavior of the lubricant mixture may result different. Indeed, the presence of air can cause the premature degradation of the lubricant and, as a consequence, increase the risk of wear of mechanical components. Moreover, aeration has a severe impact on the heat transfer capabilities of the lubricant.

The application to gearboxes of a numerical solver capable of considering the air entrainment phenomenon has not been exploited yet. The development of such a model can therefore lead to significant advancements in the field of tribology. In this work, a new solver that considers aeration was implemented in the opensource software OpenFOAM® [20]. On one hand the power losses

Published online: July 05 2022

and the aeration level predicted by the model for a single rotating spur gear were validated with experimental data in terms of resistant torque from tests with pure and aerated oil, on the other hand a back-to-back (b-t-b) test rig was studied in terms of lubricant distribution. From this analysis some interesting considerations could be made related to the impact of aeration on lubrication. Moreover, the level of aeration of rotating cylinder was also investigated. Finally, the power losses generated by a single gear rotating in water as lubricant were compared with experimental data from other authors.

2. Power Losses of Gears and Aeration Phenomenon

Two kinds of power losses can occur inside a geared transmission: load-dependent power losses, that are those associated with the transmitted load, and no-load losses, that arise because of the interaction with the fluid mixture. The no-load losses of gears are represented by the sum of three contributions: squeezing, windage and churning effect. In case of lubricant's aeration, these phenomena increase their impact on the efficiency of the transmission and, therefore, should be considered carefully.

Experimental studies on aeration were performed by LePrince et al. [21, 22], who quantified the aeration in a single stage gearbox. They concluded that the aeration increases the losses, and that the lubricant's density and viscosity alone are not enough to accurately calculate the power dissipation. Other physical properties associated with the aeration phenomenon (e.g. polar moment, surface tension and air solubility) should be considered. They proposed a heuristic approach to account for the lubricant aeration that includes some parameters that have to be determined experimentally. Subsequent studies by Neurouth et al. [23] focused on dip lubrication in high-speed gears. They analyzed several operating conditions allowing a better understanding of the aeration phenomenon in various circumstances. The higher power dissipation due to aeration is associated with the increasing energy at the interface between the air bubbles and the lubricant. They concluded that by mounting flanges at a certain distance from the gears, the aeration and the power losses can be reduced.

A numerical approach to calculate the air entrainment in a fluid was proposed by Cerne et al. [24], who developed an interface tracking algorithm based on a two-fluid model formulation [25]. Yan and Che [26] extended the work to three fluid phases. A combination of Eulerian approach and Volume of Fluid (VOF) was tested by Wardle and Weller [27]. Ma et al. [28] reformulated the source term proposed by Sene [29] to consider the turbulence intensity and applied the model to hydraulic jump [30], plunging jets [31] and flow around a ship [32]. In this paper, the aeration is implemented according to the Hirt model [33]. In this model, air is entrained into the liquid phase when the turbulent energy per unit volume are larger than the stabilizing forces of gravity and surface tension per unit volume. The expression for the source term, which is added as an explicit source term in the conservation equation of the volumetric fraction field α, is given as

$$S_g = C_{air} A_S \sqrt{2\frac{P_t - P_d}{\rho}} \,. \tag{1}$$

where S_g is the volume of air per unit of time, C_{air} is a calibration parameter, A_S the free surface area at each cell, ρ is the density, and P_t is given by

$$P_t = \rho k \tag{2}$$

being k the turbulent kinetic energy. P_t represents the turbulent forces. P_d considers the stabilizing forces and is defined as

$$P_d = \rho g_n L_T + \frac{\sigma}{L_T} \tag{3}$$

where g_n is the component of the gravity normal to the free surface, σ is the surface tension, and L_T is the turbulence characteristic length scale formulated as

$$L_T = C_\mu \sqrt{\frac{3}{2}} \frac{k^{\frac{3}{2}}}{\varepsilon} \tag{4}$$

where ε is the dissipation rate of turbulent kinetic energy and C_μ = 0.085 for the RNG k-ε turbulence model [34], which was used in the simulations. An air volume according to Eq. (1) is added to the cell in question when the turbulent forces P_t exceed the stabilizing forces P_d. The Hirt model includes the increasing of fluid volume by the addition of air and the buoyancy effects associated with entrained air. It is based on the competition between the stabilizing forces of gravity and surface tension, and the destabilizing effects of surface turbulence.

3. Experimental Setup

To compare the lubricant flow between the standard and the new implemented solver considering aeration, a standard FZG back-to-back test rig (ISO 14635-1 [35]) was taken as a reference (Fig. 1). The test section consists of two mating gears with 24 and 16 teeth, and 4.5 mm module. Conversely, the comparison with the torque measurements on this test rig was performed using the bigger gear of the test rig rotating alone. At the investigated operating conditions (rotational speed of bigger gear 150:250 RPM), the oil aeration is not significant as stated by several authors [21–23]. Therefore, in the experiments (and successively also in the numerical simulations), a preconditioning of the lubricant was made by setting the rotational speed at 3000 RPM for some seconds (which led to an aeration level of about 10%). Subsequently, the proper tests/simulations were run at the nominal rotational speeds between 150 and 250 RPM. The resistant torque was measured for three speed steps, i.e. 150 RPM, 200 RPM, 250 RPM. A KISTLER torque meter (accuracy class 0.1) was used to measure the resistant torque. The torque loss of the bearings has been determined with analytical formula (ISO 14179-1 [36]) and then subtracted from global torque measurements to isolate the net contributions of gears power losses.

From experimental observations, a cavity is created by the gear when it rotates and enters the free surface. Some of the air bubbles remain trapped between the gear's teeth, while the others circulate in the sump. Moreover, liquid impingement on the free surface occurs due to oil droplets falling into the sump contributing to the bubbles' generation.

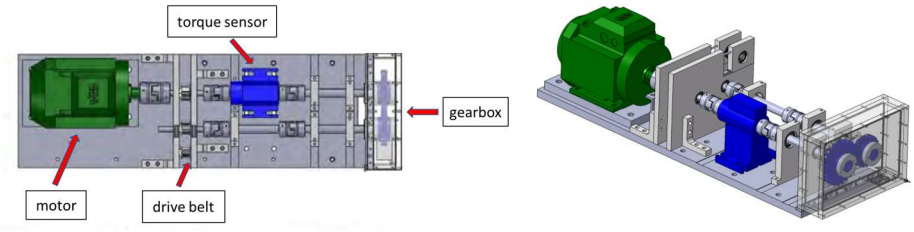

Fig. 1. Layout and schematic configuration of the considered system.

Even if the authors are aware that the determination of the amount of aeration is a very challenging engineering task, and "Air-X" sensors, which relies on low energy X-ray, are required for precise measurements, in this work the amount of aeration inside the test section was estimated by measuring the froth height and then dividing it by the initial oil level height.

4. Numerical Approach

4.1 Governing equations

CFD software packages solve the governing equations at each timestep. The simulations were considered isothermal (the energy equation was not activated), and therefore only the mass and the momentum conservation equations were solved by means of the Finite Volume method [37]. The Reynolds-Averaged Navier-Stokes (RANS) equations of mass and momentum for incompressible flows are

$$\frac{\partial \rho \langle u_i \rangle}{\partial x_i} = 0 \tag{5}$$

$$\frac{\partial \rho \langle u_i \rangle}{\partial t} + \frac{\partial \rho \langle u_i \rangle \langle u_i \rangle}{\partial x_j} = \frac{-\partial \langle \rho \rangle}{\partial x_i} + \frac{\partial}{\partial x_j}\left[\mu\left(\frac{\partial \langle u_i \rangle}{\partial x_j} + \frac{\partial \langle u_j \rangle}{\partial x_i}\right)\right] - \frac{\partial \tau_{ij}}{\partial x_i} \tag{6}$$

The Reynolds term τ_{ij} is expressed with the eddy viscosity hypothesis μ_t

$$-\tau_{ij} = \mu_t\left(\frac{\partial \langle u_i \rangle}{\partial x_j} + \frac{\partial \langle u_j \rangle}{\partial x_i}\right) - \frac{2}{3}\rho\delta_{ij}k \tag{7}$$

$$\mu_t = C_\mu \rho \frac{k^2}{\varepsilon} \tag{8}$$

Turbulence was modeled according the RNG k-ε model since it improves accuracy in rotating flows [34]. The conservation equations of the turbulence kinetic energy (k) and the dissipation rate (ε) are

$$\frac{\partial}{\partial t}(\rho k) + \frac{\partial}{\partial x_i}(\rho k u_i) = \frac{\partial}{\partial x_j}\left[\alpha_k \mu_{eff}\frac{\partial k}{\partial x_j}\right] + G_k + G_b - \rho\varepsilon - Y_M + S_k \tag{9}$$

$$\frac{\partial}{\partial t}(\rho \varepsilon) + \frac{\partial}{\partial x_i}(\rho \varepsilon u_i) = \frac{\partial}{\partial x_j}\left[\alpha_\varepsilon \mu_{eff}\frac{\partial k}{\partial x_j}\right] + \frac{C_{1\varepsilon}\varepsilon}{k}(G_k + C_{3\varepsilon}G_b) - \frac{C_{2\varepsilon}\rho\varepsilon^2}{k} - R_\varepsilon + S_\varepsilon \tag{10}$$

In order to solve the multiphase physics, the VOF method [38] is applied. In this method, the averaged properties ψ (such as density and viscosity) are used to describe the properties of an equivalent fluid in every computational cell as follows

$$\psi = \psi_1 \alpha + \psi_2(1-\alpha) \tag{11}$$

where ψ represents the considered property of the fluid, α is the volumetric fraction, and the subscripts 1 and 2 stand for the two fluids (in this case air and oil). Moreover, the MULES [1] correction was added in the solver algorithm in order to obtain a more stable and bounded solution of the volumetric fraction. This is achieved by adding a dummy velocity field (u_C) (relative velocity that acts as a velocity perpendicular to the interface) in the conservation equation of the volumetric fraction

$$\frac{\partial \alpha}{\partial t} + \nabla(\alpha u) + \nabla(u_C \alpha(1-\alpha)) = 0 \tag{12}$$

To account for cavitation, the equation becomes

$$\frac{\partial \alpha}{\partial t} + \nabla(\alpha u) + \nabla(u_C \alpha(1-\alpha)) = \frac{\dot{m}}{\rho_v} \tag{13}$$

being m over dot the mass transfer and ρ_v the vaporization pressure. A phase change model must be introduced. The most used in CFD are those by Kunz [39], Merkl [40] and Saurer [41]. For monophasic operating conditions (as a gearbox completely immersed in oil), cavitation models allow to account for the phase change (vaporization). For what concerns the biphasic modeling (as oil-air),

aeration plays a role especially at high rotational speeds, and must be considered in the numerical model for a more accurate prediction of real physics. This is done by adding a source term in volumetric fraction equation

$$\frac{\partial \alpha}{\partial t} + \nabla(\alpha u) + \nabla(u_c \alpha(1-\alpha)) = S_g \tag{14}$$

where S_g is calculated from Eq. (1). The coefficient of proportionality C_{air} in the equation of the source term is set to 0.5. This value was used by Hirt [33] for many test cases. He concluded that this value can be reasonable for most of the applications, as on average it is assumable that air will be entrained over about half the surface area. This value has been used in all validation tests by Hirt.

The implemented solver was initially applied to a simple geometry in order to verify if it behaves according to what it is expected. The test case consisted in a free surface and an ejection nozzle. The problem was modelled as 2D (a square with dimensions of 0.5x0.5 m^2). The domain was meshed with quadrilateral elements. An inlet velocity of 0.4 m/s is applied at the jet patch, while the pressure is assigned a Neumann boundary condition. The two phases are air and water at ambient temperature. As it can be seen from Fig. 2, while with standard multiphase solver the interface between the liquid (water) and the gas is sharp, the new solver promotes a smoother transition at the interface. The low gradient of volume fraction indicates that significant amount of air remains entrapped in the liquid. This means that, at least qualitatively, the physics of the problem is captured from the solver. Moreover, the velocity arrows clearly indicate that in the case of the standard multiphase solver the jet significantly penetrates the steady sump, while the new solver and the related foaming effects slow down the main flow that diffuses radially. As shown in the next paragraphs, this effect (air entrapment) occurs each time the free surface is broken by a jet/impact with a droplet of liquid.

4.2 Initialization of the Solution and Simulation of the Nominal Conditions

Considering that the aeration of an oil sump has a large time scale, the preconditioning of the lubricant (i.e. the generation of the air trapping that experimentally is made by rotating the gear at 3000 RPM for a short time just before the real measurement at the nominal speed) is made in the numerical models similarly: the preliminary simulations at 3000 RPM were performed exploiting a semi-transient approach, namely the MRF (Multi Reference Frame) [42]. The MRF approach foresees a moving reference frame and a "frozen" geometry. While the numerical transitory does not strictly represent the physical transitory, the method has the advantage of reaching the regime condition (also for large time scales) in a very fast way. Once the regime was initialized by the MRF approach, a transient solver takes over and simulates the nominal conditions.

As previously mentioned, three different systems were studied: two mating gears, single rotating gear (two different geometries), and single rotating disk. While the last system could be modelled by means of a static mesh, the configurations involving gears required advanced mesh handling strategies. Specifically, the sliding mesh approach was used for the single gear configurations and the Global Remeshing Approach (GRA) for the back-to-back test rig where mating gears are present.

4.2.1 Global Remeshing Approach (GRA)

The GRA exploits a 2.5D extrusion algorithm (implemented in the preprocessor Salome [43]) that reduces the computational effort of the mesh generation compared to a full 3D tetrahedral mesh generation. In Fig. 3 the mesh of the computational domain is shown. The mesh has a maximum non-orthogonality of 35 and a maximum skewness below 1. The good quality of the mesh is mainly due to the meshing algorithm which exploits prismatic elements rather than tetrahedrons. The simulation process is based on a mesh-to-mesh interpolation of the results which follows the boundaries' rotations. When the physical quantities are stabilized and the regime condition is reached, the results are post-processed. This approach has been previously used by the authors providing very good results compared to experiments [44].

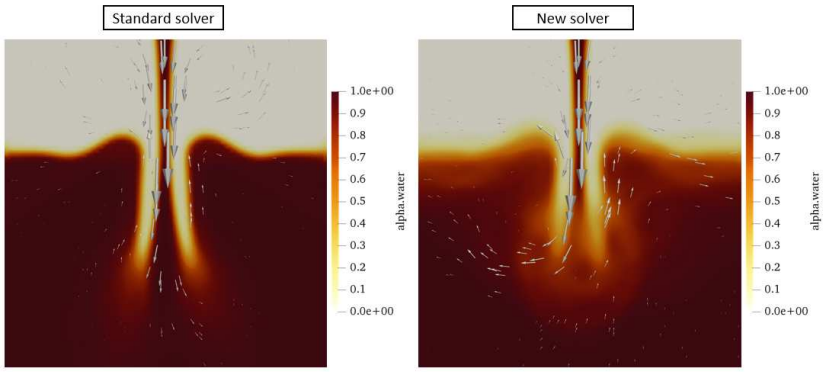

Fig. 2. Test case: distribution of the volumetric fraction in case of standard multiphase solver (left) and new solver that considers aeration (right).

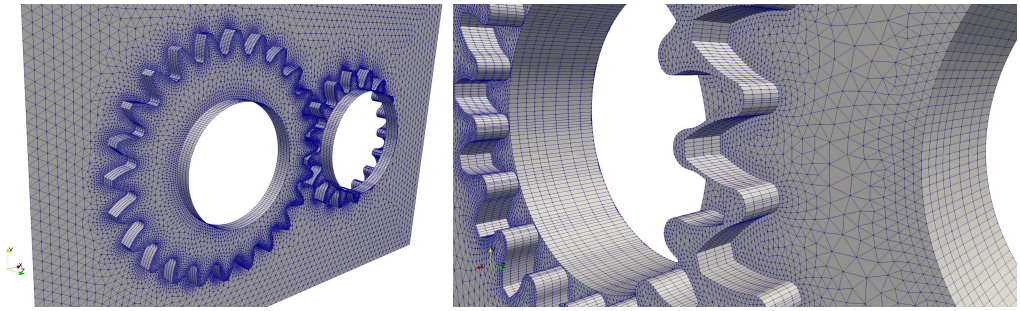

Fig. 3. Numerical mesh and detailed view in the meshing region.

In order to accomplish the deformation of the boundaries, the Laplace smoothing equation was used

$$\nabla(\gamma \nabla u) = 0 \tag{15}$$

where γ represents the diffusivity (parameter that affects the mesh distortion) and u the grid deformation velocity such that

$$x^{i+1} = x^{i} + \Delta t \cdot u \tag{16}$$

where x represents the position of the nodes of the mesh and t the actual timestep. With such approach, the mesh deformation is not uniformly distributed in the computational domain. Indeed, it is larger in the region near the moving boundaries and lower as the mesh points are in the static region of the grid.

4.2.2 Sliding Mesh Approach

To describe the kinematics of a single rotating gear, the sliding mesh approach [45] was used. The sliding mesh approach is based the creation of different cell zones (usually a stationary domain and one or more rotational domains). The problem of non-conformal grids can be overcome thanks to Arbitrary Mesh Interfaces (AMI). In fact, the domains can be stitched together even if the mesh nodes are not coincident, since the AMI acts as a numerical connector on both sides of the interface. In this case, the static domain is represented by the box, while the dynamic domain, which rotates, is composed by the cells inside the cylindrical partition (Fig. 4). Both domains have been discretized with a native utility of OpenFOAM® called *snappyHexMesh* that needs a pure hexahedral mesh as background (created with *blockMesh*) and the STL files of the patches to snap (in this case the gear and the cylindrical partition). The final mesh is made of hexahedral elements mainly.

While the data of the back-to-back test rig were reported in chapter 3, the additional simulations with water as lubricant were performed with the geometry from LePrince et al. [21], whose gear has a 3 mm module, 53 teeth and a 24 mm face width. The domain and the discretization are shown in Fig. 5.

4.2.3 Static Mesh

For the simulation of the smooth disk (diameter of 120 mm), no particular mesh handling strategies were required. The rotational speed of the disk was imposed by means of a velocity boundary condition without the need of moving the boundary elements. The domain was discretized with hexahedral elements (Fig. 6).

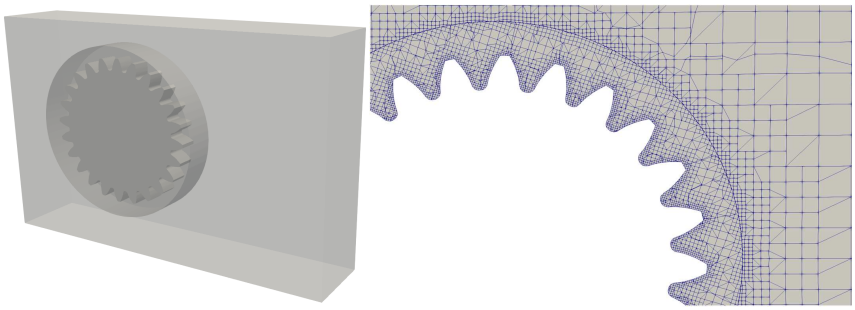

Fig. 4. Geometrical domain and detail of the numerical mesh near the wheel.

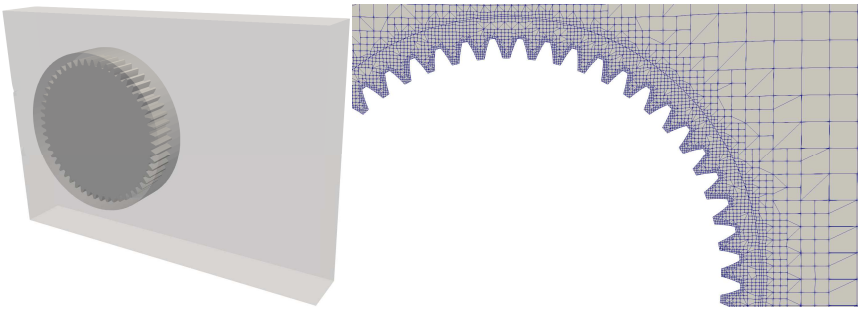

Fig. 5. Geometrical domain and detail of the numerical mesh near the wheel.

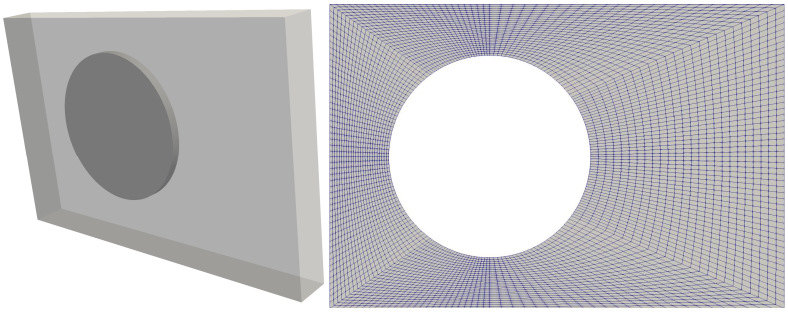

Fig. 6. Geometrical domain and numerical mesh of the smooth disk. The domain was properly partitioned to obtain a full structured mesh.

Table 1. Summary of the investigated operating conditions.

Configuration	Meshing strategy	Tangential velocity [m/s]	Lubrication	Target		
				Lubricant distribution	Aeration level	Torque
b-t-b 2 gears	**Remeshing**	0.86	Centerline Nytex 810 20 °C	✓		
	Remeshing	1.14		✓		
	Remeshing	1.52		✓		
b-t-b 1 gear	**Sliding mesh**	0.86	Centerline Nytex 810 20 °C		✓	✓
	Sliding mesh	1.14			✓	✓
	Sliding mesh	1.52			✓	✓
LePrince 1 gear	**Sliding mesh**	33.28	Relative immersion 0.5 Water 50 °C			✓
	Sliding mesh	41.60				✓
	Sliding mesh	49.92				✓
Disk	**Static mesh**	18.84	Centerline Nytex 810 20 °C		✓	

Table 2. Oil and water characteristics.

	Nytex 810	Water
Characteristics	**Value**	
Viscosity ν, 40 °C	22.4 mm^2/s	0.65 mm^2/s
Viscosity ν, 100 °C	3.7 mm^2/s	0.29 mm^2/s
Density ρ, 15 °C	901 kg/m^3	999 kg/m^3

4.3 Assumptions of the numerical models

The assumptions of the CFD models are summarized hereafter.

1. The energy equation was not activated. The properties of the fluids were set based on the operating temperature, which was kept almost constant in the experiments.
2. The bearings were not modelled. This assumption is consistent with the experiments since the bearing power losses were subtracted from the total power losses in order to isolate the contribution of the gears. However, it must be noted that the loss torque determined by subtracting the bearing losses (calculated analytically) from the total no-load loss (measured) may introduce a source of uncertainty.
3. The geometry of the housing and the gears are the same of the experimental tests. However, the micro-geometrical parameters of the gears have not been considered in the CAD model. This is not expected to have a significant impact on the oil flow and power losses.
4. For the simulation of two meshing gears, the gears have been scaled to 99% of their size in order to avoid poor element quality and numerical singularities in the very small gap between the tooth flanks. This assumption is actually required for all mesh based CFD simulations.

The assumptions of the numerical models seem to be consistent with the experimental operating conditions. The results of the simulations are discussed in paragraph 5.

4.4 Solver Settings

The PIMPLE algorithm was used. A convergence criterion of $1x10^{-6}$ was set to all field's variables. The pressure was solved with the PCG (Preconditioned Conjugate Gradient) solver, while the PBiCG (Stabilized preconditioned bi-conjugate gradient) was adopted for the velocity. To obtain a stable simulation a maximum Courant number of 1 was imposed. The first order implicit Euler scheme was utilized to discretize the time derivative, while the second order linearUpwind scheme and the vanLeer scheme were exploited for the velocity and the convection of the volumetric fraction, respectively. The convective fluxes in the turbulence equations were discretized using second order schemes.

5. Results

Several operating conditions were studied with the standard multiphase solver and the new developed one that considers the aeration. The GRA was used to investigate the differences of two mating gears, while the sliding mesh approach was used to validate losses and the amount of air entrapped in the lubricant (level of aeration). The possibility to test different mesh handling algorithms was useful to understand the stability and flexibility of the new solver as well as its computational effectiveness. In Table 1 the approaches as well the targets of the investigation are reported.

The lubricants are Nytex 810 and water, whose main physical properties are exposed in Table 2. The properties at the experimental operating temperatures θ were calculated as

$$\rho_\Theta = \left(\frac{\rho_{15}}{1000} - (\Theta - 15)\cdot 0.0007\right)\cdot 1000 \tag{17}$$

$$\nu_\Theta = \nu_{40} + \left(\frac{\Theta - 313}{60}\right)\cdot(\nu_{100} - \nu_{40}) \tag{18}$$

5.1 Oil Distribution

The GRA was exploited to study the difference between the solvers in terms of lubricant distribution. In Fig. 7 the comparison of the volumetric fraction for the three angular velocities on the symmetry plane is reported. As it can be noticed, the oil distribution changes as the rotational speed increases and the lubricant starts to splash in the gearbox.

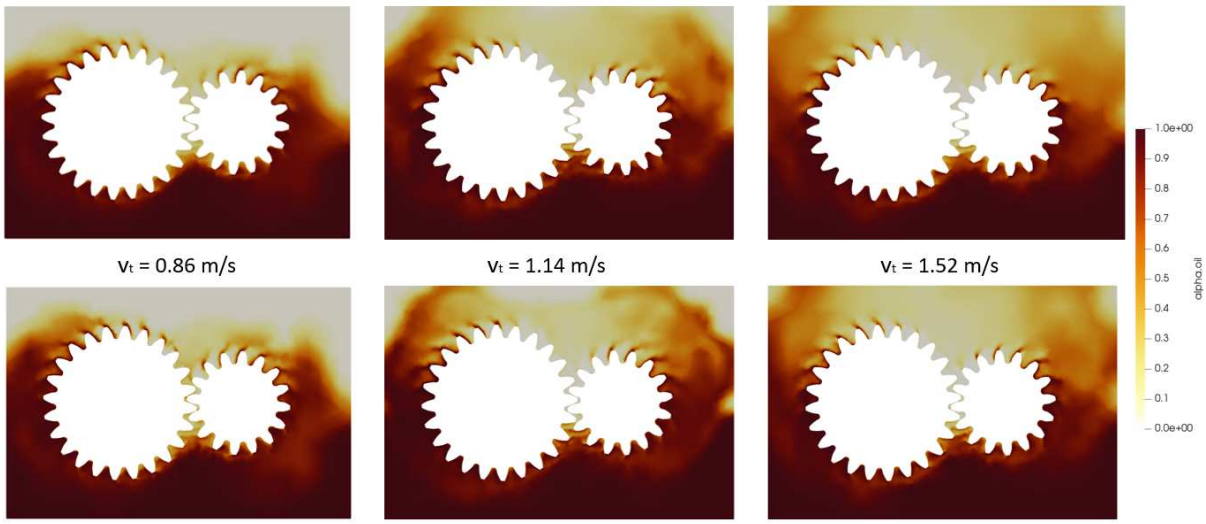

Fig. 7. Standard multiphase solver (top row) and new solver that consider aeration (bottom row) volumetric fraction for the different tangential velocities.

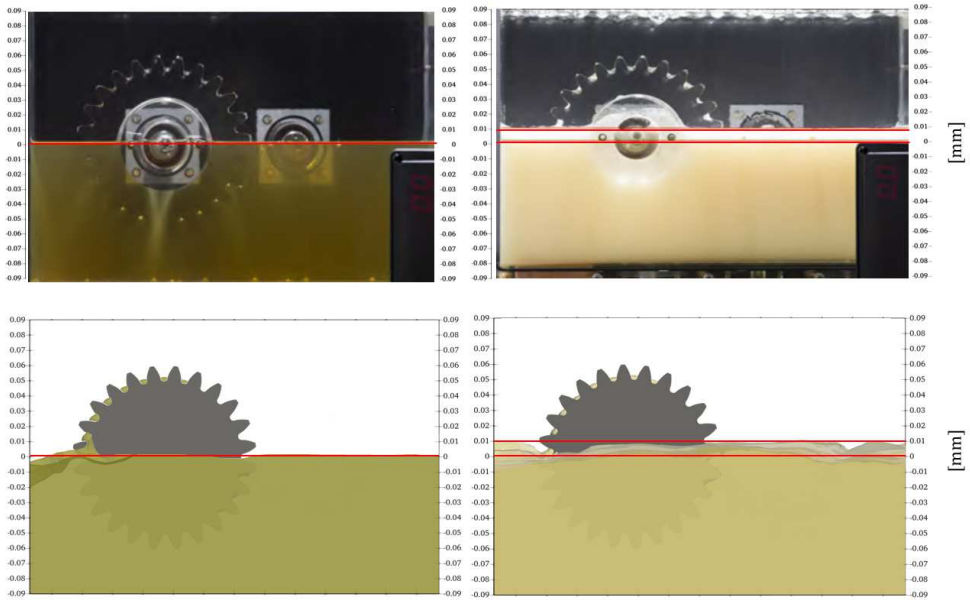

Fig. 8. Experimental (top row) and numerical (bottom row) lubricant level in the non-aerated and aerated configuration ($0 < \alpha < 0.66$).

It is possible to appreciate the effect of the new implemented solver. Indeed, there are regions, especially below the wheels, with higher air concentration in the oil phase with respect to the standard solver (a behavior that was observed also in the test case explained in chapter 4). The aerated condition seems to increase the splashing phenomenon of the oil. This might be one of the causes of the increased churning losses for the aerated configuration.

In order to estimate the aeration level, the wheel's rotation was stopped at regime condition so that the mixture could drop. By doing so, only the effect of gravity was simulated. It is expected that the level of the mixture will be higher due the air entrainment in the lubricant. In Fig. 8 the experimental and the simulation results in terms of lubricant level are shown (after the gear was slowed down to zero). As expected, in the aerated configuration the lubricant level is higher compared to the non-aerated one. Therefore, the new solver behaves correctly and seems to be able to describe the physics involved when the aeration is considered. The values of α have been divided in 3 ranges: from 0 to 0.33 (pure oil), from 0.33 to 0.66 (oil and foaming effects), from 0.66 to 1 (pure air). The plotted lubricant level ranges therefore from 0 to 0.66 in order to account for the possible foaming effects.

This figure indicates that the new implemented solver seems to behave as intended and to model the physics of aeration inside a gearbox. In fact, the free surface level is higher in the aerated configuration due the higher volume occupied by the mixture, i.e. the volume increment associated to the air entrainment in the oil. The experimental estimation of aeration level is about 10% resulting in 9 mm higher free surface level, while in the simulations it is estimated to be 11% resulting in 10 mm higher free surface level.

The same methodology was applied to study the aeration of a rotating cylinder instead of a gear. In this case, the aeration is higher with respect to the gear. In fact, it results in 20 mm higher than the centerline and, therefore, in 20% aeration estimation. The comparison between experimental and simulated condition are shown in Fig. 9.

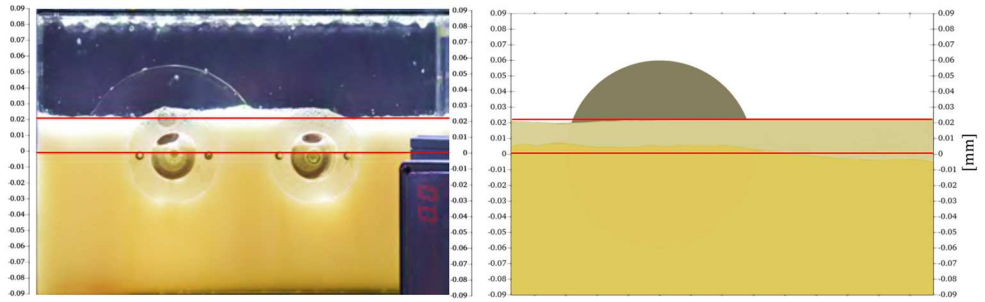

Fig. 9. Experimental and simulated lubricant level in the aerated configuration for a disk.

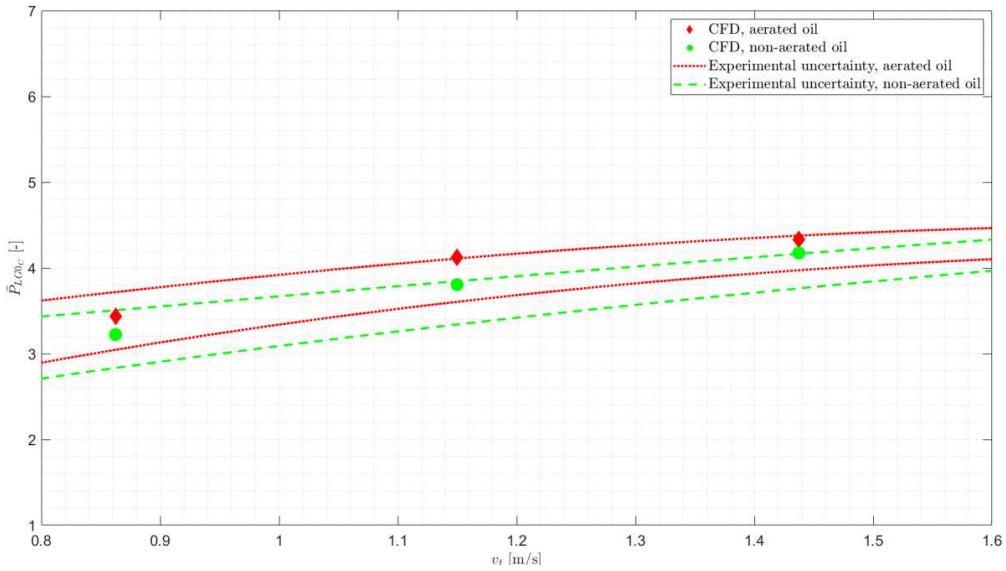

Fig. 10. Non-dimensional power losses vs tangential velocity for the three studied configurations with oil as lubricant.

5.2 Analysis of the Power Losses

The calculation of the power losses is based on a developed utility that reads the pressure and velocity fields at each timestep and computes the inertial and viscous contribution of the losses at all the timesteps. While in the transitory the forces have significant fluctuations, at regime they fluctuate around a mean value at the gear meshing frequency. Considering the timesteps of every complete engagement, the comparison between successive averages indicates whether or not the forces are stabilized. When less than 5% difference was observed, the solution was considered stabilized and the results postprocessed. The calculation of the torque implemented in the utility is

$$T = \sum_i \left(r_i \times F_{pi} + r_i \times F_{ri} \right)_i \tag{19}$$

where r_i is the distance of the *i-th* cell's center from the specified rotational axis and F_{pi} and $F_{\tau i}$ are the pressure and the viscous force vectors. The power loss is then obtained by multiplying the torque by the angular velocity of the wheel. The power losses have been non-dimensionalized as

$$\bar{P} = \frac{P}{\frac{1}{2} r_p^3 \rho \omega S_m} \tag{20}$$

where P over sign is the non-dimensional power loss, P is the actual power loss, r_p is the pitch radius, ρ is the density, ω is the rotational speed of the wheel, S_m is the immersed area of the gear at rest.

5.2.1 Oil as Lubricant

Figure 10 shows the experimental and the predicted values of non-dimensional power losses vs tangential velocity in case of the standard and aerated configuration.

Both simulations with the standard and the new solver fit within the range of the experimental uncertainties (for which 2 series of data are available). This highlights the great potential of this tool to predict the losses in presence of aerated lubricants. The aerated configuration shows an increase in the losses about 5%.

The numerical simulations allowed also to distinguish between pressure and viscous contribution. As expected, the inertial forces are predominant and represent most of the total losses. This highlights that the density is a much more influencing parameter than viscosity and, therefore, should be considered carefully in the design of mechanical gearboxes. Figure 11 shows the different contribution of pressure and viscous effects. It emerges that the aeration further reduces the shear of the viscous losses by affecting the mixture viscosity and density differently. This observation could be probably explained considering that an aeration of 10% implies a reduction of the viscosity of the mixture and at the same time a specific volume increase. Consequently, the viscous

losses reduce, and the inertial ones increase. For the lowest rotational speed, the new shear (1.12%-98.88%) predicted by the numerical simulation considering aeration are approximately related to a 10% reduction of the viscous losses and a 10% increase of the inertial ones with respect to the reference configuration (1.36%-98.64%). This is interesting considered that the measured level of aeration was 10%. For the other two velocities, a reduction of the viscous losses and an increase of the inertial ones about 15% is predicted.

5.2.2 Water as Lubricant

In order to verify the accuracy of the solvers for different fluids, the power losses of a spur gear (3 mm module, 53 teeth and 24 mm face width) partially immersed in water were studied. Figure 12 reports the comparison between experimental data from LePrince et al. [21] and the simulated results in terms of non-dimensional power losses and tangential velocity. As it can be noticed, the standard solver underestimates the power losses, even if it can predict the main trend. Instead, the new solver fit better the experimental data (represented with a confidence interval of 10% from the mean value) and, therefore, represents an improvement of the existing available approaches. This points out the importance of choosing the right solver for a better representation of the problem of interest.

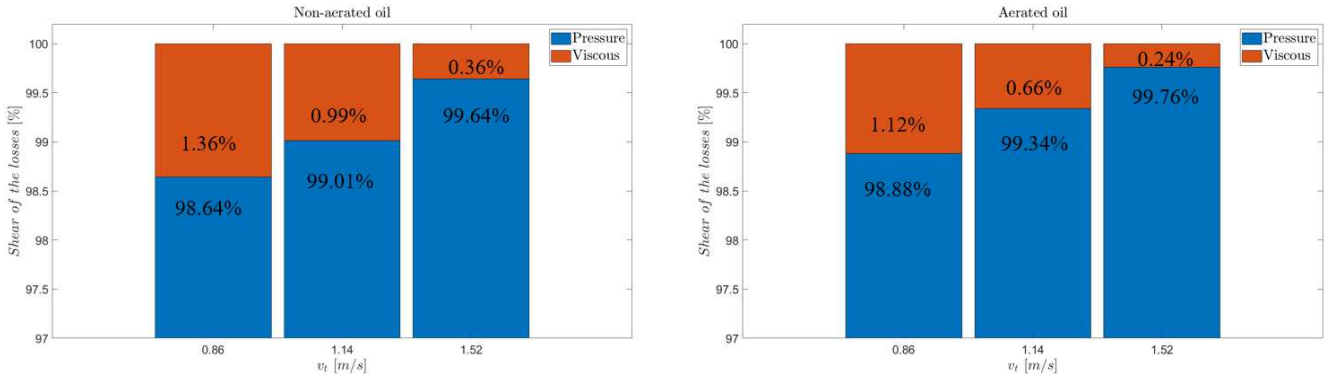

Fig. 11. Pressure and viscous contribution to the total losses in non-aerated and aerated configurations with oil as lubricant.

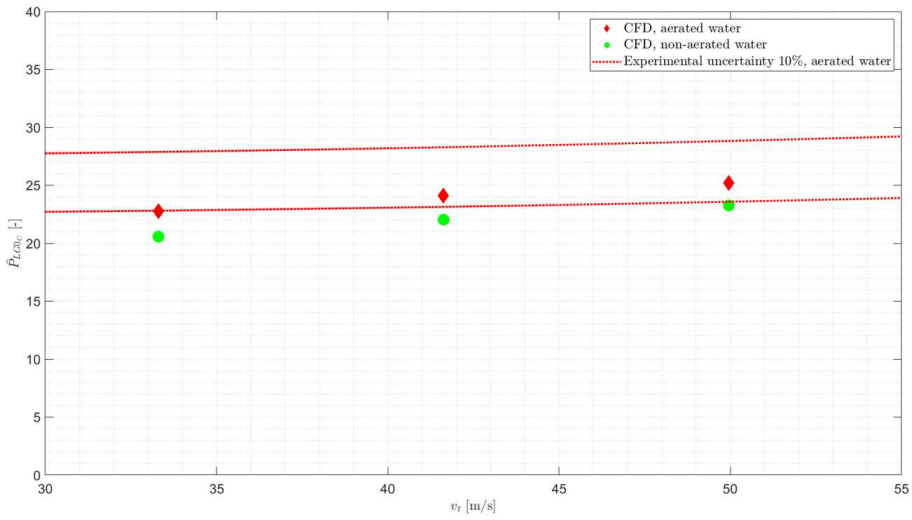

Fig. 12. Churning power losses vs rotational speed with water as fluid.

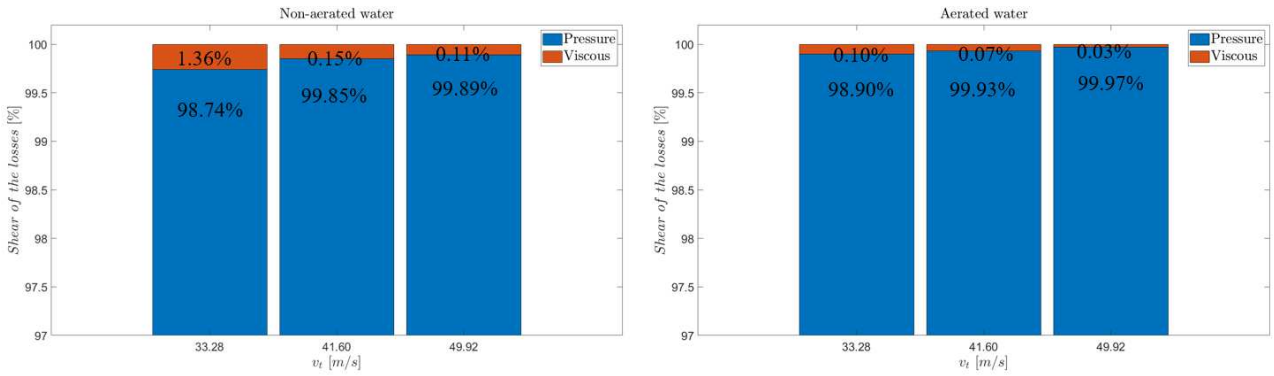

Fig. 13. Pressure and viscous contribution to the total losses in non-aerated and aerated configurations with water as lubricant.

Also in the case of water, the inertial forces are of higher orders of magnitude with respect to the viscous one (Fig. 13). Moreover, it could be appreciated that for very high tangential velocities the shear of the viscous losses approximates zero. The decrease is more than linear but in both aerated and non-aerated conditions the decrease rate is comparable: the shear decrease of about -30% for the 41.6 m/s velocity with respect to the 33.28 m/s velocity (v_t +25%), and about -70% for the 49.92 m/s with respect to the 33.28 m/s (v_t +50%).

6. Discussion

Differently from previous studies, a new solver that considers the air entrainment in the lubricant was applied to the simulation of gearboxes. The comparison of the oil fluxes inside the transmission highlighted the importance to use an appropriate solver to capture the real physics of the problem. The high customization possibility of the opensource software OpenFOAM® allows engineers to develop dedicated libraries and specific solvers able to increase the accuracy of the numerical simulations. In this paper, the losses in the normal and aerated configuration as well as the amount of air entrapped were validated numerically. This opens new possibilities in the simulation of lubricated mechanical systems. The application to gearboxes of a solver that accounts for the aeration level in the lubricant, and the comparison of flows and power losses has been never reported before.

The adoption of a numerical solver that considers the air entrainment in the lubricant can represent a significant advancement in the field of tribology. In fact, some differences in the oil distribution were observed. These differences were also present in terms of power losses that increased as a consequence of the foaming effects. This new solver allows a better representation of the physical phenomenon that occurs when air bubbles are generated. Different mesh handling strategies were used demonstrating its flexibility with different grids' motion algorithms. The validation of the results in the tested conditions was fundamental to understand the accuracy and behavior of the new solver in case of aeration. The computational cost of the new solver did not differ significantly from the standard multi-phase solver, resulting in a comparable simulation time.

For what concerns the differences between the experimental and the simulations results, the experimental measurements always involve measuring uncertainties, e.g. due to the relative error of the loss torque meter and due to the shafts imbalance. Moreover, the bearing losses have been calculated analytically and then subtracted from the total power losses. This could be another source of uncertainty. Regarding the numerical models, some simplifications as the micro-geometrical parameters of the gears could influence the results as well. In any case, it should be noted that the numerical values are comprised in the 10% confidence interval with respect to the experimental data.

7. Conclusions

The introduction of CFD to the study of gearboxes allowed engineers to overcome the limitations of the analytical models. These are in fact limited by the configuration of the tests and cannot be extended to more complex geometries. Nowadays, CFD software can solve dynamic multiphase simulations with different approaches. While the challenge of handling the topological changes of the computational domain was recently solved, the simulation of more complex physics phenomena like cavitation and aeration is still not available or could be further improved. In this paper, the aeration phenomenon in the lubricant was considered thanks to a new implemented solver. The losses were validated for the standard and for the aerated lubricant configuration, demonstrating the accuracy of the new implemented solver. Moreover, the simulations allowed also to separate the inertial from the viscous contribution to the total losses. The inertial losses are of a different order of magnitude with respect to the viscous ones. The comparison of the oil distribution showed a higher concentration of air in the aerated configuration, thus demonstrating the effects on the mixture of the new solver.

The new solver can be possibly used to study lubricated mechanical components in general. Its increased accuracy provides the user with advanced modeling possibilities making it ideal in the early stages of the design phase to evaluate the impact on the performance of the system or even to better understand what the local behavior of the lubricant inside the system is. The solver showed high flexibility and compatibility with different mesh motion strategies. This allows engineers to adapt the simulation model to the specific case of interest. In future it is planned to apply the solver to different kinematics, e.g., bearings, planetary gear and cycloidal architectures.

Author Contributions

M.N. Mastrone implemented the multiphase solver and the numerical models; M.N. Mastrone and F. Concli analyzed the results. The manuscript was written through the contribution of all authors. All authors discussed the results, reviewed, and approved the final version of the manuscript.

Acknowledgments

Not applicable.

Conflict of Interest

The authors declared no potential conflicts of interest concerning the research, authorship, and publication of this article.

Funding

The authors received no financial support for the research, authorship, and publication of this article.

Data Availability Statements

The datasets generated and/or analyzed during the current study are available from the corresponding author on reasonable request.

Nomenclature

g	Gravitational acceleration [m/s^2]	α	Volumetric fraction [-]
p	Pressure [Pa]	ρ	Density [kg/m^3]
k	Turbulent kinetic energy [m^2/s^2]	ω	Rotational speed [rad/m^3]
ε	Dissipation rate [m^2/s^3]	L_T	Turbulence characteristics length [m]
υ	Kinematic viscosity [m^2/s]	P_d	Stabilizing forces [kg/m-s^2]
μ	Dynamic viscosity [kg/m-s]	P_t	Turbulent forces [kg/m-s^2]

References

[1] Rusche, H., *Computational Fluid Dynamics of Dispersed Two-Phase Flows at High Phase Fractions*, Ph.D. Thesis, Imperial College of Science, Technology and Medicine, London, 2002.
[2] Ubbink, O., *Numerical prediction of the two fluid systems with sharp interfaces*, Ph.D. Thesis, University of London, London, 1997.
[3] Lu, F., Wang, M., Bao, H., Huang, W. and Zhu, R., Churning power loss of the intermediate gearbox in a helicopter under splash lubrication, *Proceedings of the Institution of Mechanical Engineers, Part J: Journal of Engineering Tribology,* 236(1), 2022, 49-58.
[4] Lu, F., Wang, M., Pan, W., Bao, H. and Ge, W., CFD-based investigation of lubrication and temperature characteristics of an intermediate gearbox with splash lubrication, *Applied Sciences,* 11(1), 2020, 352.
[5] Bianchini, C., Da Soghe, R., Giannini, L., Fondelli, T., Massini, D., Facchini, B. and D'Errico, J., Load independent losses of an aeroengine epicyclic power gear train: Numerical investigation, *ASME Turbo Expo,* Phoenix, Arizona, USA, GT2019-91309, 2019.
[6] Bianchini, C., Da Soghe, R., Errico, J. D. and Tarchi, L., Computational analysis of windage losses in an epicyclic gear train, *ASME Turbo Expo,* Charlotte, NC, USA, GT2017-64917, 2017.
[7] Li, J., Qian, X. and Liu, C., Comparative study of different moving mesh strategies for investigating oil flow inside a gearbox, *International Journal of Numerical Methods for Heat & Fluid Flow,* 2022, doi: 10.1108/HFF-10-2021-0695.
[8] Liu, H., Jurkschat, T., Lohner, T. and Stahl, K., Detailed investigations on the oil flow in dip-lubricated gearboxes by the finite volume CFD method, *Lubricants,* 6(2), 2018, 47.
[9] Liu, H., Link, F., Lohner, T. and Stahl, K., Computational fluid dynamics simulation of geared transmissions with injection lubrication, *Proceedings of the Institution of Mechanical Engineers, Part C: Journal of Mechanical Engineering Science*, 233(21-22), 2019, 7412–7422.
[10] Mastrone, M. N. and Concli, F., CFD simulation of grease lubrication: Analysis of the power losses and lubricant flows inside a back-to-back test rig gearbox, *Journal of Non-Newtonian Fluid Mechanics,* 297, 2021, 104652.
[11] Mastrone, M. N. and Concli, F., A Multi Domain Modeling Approach for the CFD Simulation of Multi-Stage Gearboxes, *Energies,* 15(3), 2022, 837.
[12] Mastrone, M. N. and Concli, F., CFD simulations of gearboxes: implementation of a mesh clustering algorithm for efficient simulations of complex system's architectures, *International Journal of Mechanical and Materials Engineering,* 16(1), 2021, 1-19.
[13] Močilan, M., Husár, Š., Labaj, J. and Žmindák, M., Non-stationary CFD Simulation of a Gear Pump, *Procedia Engineering*, 177, 2017, 532–539.
[14] Gao, G., Yin, Z., Jiang, D. and Zhang, X., Numerical analysis of plain journal bearing under hydrodynamic lubrication by water, *Tribology International,* 75, 2014, 31–38.
[15] Sawicki, J. and Rao, T., Cavitation Effects on the Stability of a Submerged Journal Bearing, *International Journal of Rotating Machinery,* 10(3), 2004, 227-232.
[16] Riedel, M., Schmidt, M. and Stücke, P., Numerical investigation of cavitation flow in journal bearing geometry, *EPJ Web of Conferences,* 45, 2013.
[17] Del Campo, D., Castilla, R., Raush, G. A., Gamez Montero, P. J. and Codina, E., Numerical analysis of external gear pumps including cavitation, *Journal of Fluids Engineering,* 134(8), 2012, 081105.
[18] Maccioni, L., Chernoray, V. G., Bohnert, C. and Concli, F., Particle Image Velocimetry measurements inside a tapered roller bearing with an outer ring made of sapphire: design and operation of an innovative testrig, *Tribology International,* 165, 2022, 107313.
[19] Maccioni, L., Chernoray, V. G., Mastrone, M. N., Bohnert, C. and Concli, F., Study of the impact of aeration on the lubricant behavior in a tapered roller bearing: innovative numerical modelling and validation via particle image velocimetry, *Tribology International,* 165, 2022, 107301.
[20] OpenFOAM. Available online: http://www.openfoam.com.
[21] Leprince, G., Changenet, C., Ville, F., Velex, P. and Jarnias, F., Influence of oil aeration on churning losses, *Proceedings of the JSME International Conference on Motion and Power Transmissions,* 463-468, 2009.
[22] Leprince, G., Changenet, C., Ville, F., Velex, P., Dufau, C. and Jarnias, F., Influence of aerated lubricants on gear churning losses–an engineering model, *Tribology Transactions,* 54(6), 2011, 929–938.
[23] Neurouth, A., Changenet, C., Ville, F., Octrue, M. and Tinguy, E., Experimental Investigations to Use Splash Lubrication for High-Speed Gears, *Journal of Tribology,* 139(6), 2017, 061104.
[24] Cerne, G., Peterlin, S. and Tiselj, I., Coupling of the Interface Tracking and the Two-Fluid Models for the Simulation of Incompressible Two-Phase Flow, *Journal of Computational Physics,* 171(2), 2001, 776–804.
[25] Drew, D. and Passman, S., *Theory of Multicomponents Fluids,* Springer, Science & Business Media, New York, 2006.
[26] Yan, K. and Che, D., A coupled model for simulation of the gas - liquid two-phase flow with complex flow patterns, *International Journal of Multiphase Flow,* 36(4), 2010, 338–348.
[27] Wardle, K. E. and Weller, H. G., Hybrid Multiphase CFD Solver for Coupled Dispersed / Segregated Flows in Liquid-Liquid Extraction, *International Journal of Chemical Engineering,* 2013, 2013, 128936.
[28] Ma, J., Oberai, A., Drew, D., Lahey, R. and Moraga, F., A quantitative sub-grid air entrainment model for bubbly flows – plunging jets, *Computers and Fluids,* 39(1), 2010, 77–86.
[29] Sene, K. J., Air entrainment by plunging jets, *Chemical Engineering Science,* 43(10) 1988, 2615–2623.
[30] Ma, J., Oberai, A., Drew, D., Lahey, R. and Moraga, F., Modeling Air Entrainment and Transport in a Hydraulic Jump using Two-Fluid RANS and DES Turbulence Models, *Heat and Mass Transfer,* 47(8), 2011, 911–919.
[31] Ma, J., Oberai, A., Drew, D., Lahey, R. and Moraga, F., A comprehensive sub-grid air entrainment model for RaNS modeling of free-surface bubbly flows, *The Journal of Computational Multiphase Flows,* 3(1), 2011, 41–56.
[32] Ma, J., Oberai, A., Drew, D., Lahey, R. and Moraga, F., Two-Fluid Modeling of Bubbly Flows around Surface Ships Using a Phenomenological Subgrid Air Entrainment Model, *Computers and Fluids,* 52, 2011, 50–57.
[33] Hirt, C. W., Modeling Turbulent Entrainment of Air at a Free Surface, *Flow Science, Inc.,* 2003.
[34] Yakhot, V., Orszag, S., Thangam, S., Gatski, T. and Speziale, C., Development of turbulence models for shear flows by a double expansion technique, *Physics of Fluids A: Fluid Dynamics,* 4(7), 1992, 1510–1520.
[35] *International Organization for Standardization*, ISO 14635-1, FZG test method A/8,3/90 for relative scuffing load-carrying capacity of oils, 14635-1, International Organization for Standardization: Geneva, Switzerland, 2000.
[36] *International Organization for Standardization*, ISO 14179-1, Gears – Thermal capacity – Part 1: Rating gear drives with thermal equilibrium at 95 °C sump temperature, 14179-1, International Organization for Standardization: Geneva, Switzerland, 2001.
[37] Versteeg, H. K. and Malalasekera, W., *An Introduction to Computational Fluid Dynamics—The Finite Volume Method*, Pearson, London, 2007.
[38] Hirt, C. W. and Nichols, B. D., Volume of fluid (VOF) method for the dynamics of free boundaries, *Journal of Computational Physics,* 39(1), 1981, 201–225.
[39] Kunz, R. F., Boger, D. A., Stinebring, D. R., Chyczewski, T. S., Lindau, J. W., Gibeling, H. J. and Govindan, T. R., Preconditioned Navier-Stokes Method for Two-Phase Flows with Application to Cavitation Prediction, *Computers and Fluids,* 29(8), 2000, 849–875.
[40] Merkle, C. L., Computational Modeling of the Dynamics of Sheet Cavitation, *3rd International Symposium on Cavitation,* Grenoble, France, 1998, 1998.
[41] Saurer, J., *Instationären kavitierende Strömung - Ein neues Modell, basierend auf Front Capturing (VoF) and Blasendynamik*, Ph.D. Thesis, Faculty of Machine Design, Universität Karlsruhe, Karlsruhe, 2000.
[42] Silva, P. A., Tsoutsanis, P. and Antoniadis, A. F., Simple multiple reference frame for high-order solution of hovering rotors with and without ground effect, *Aerospace Science and Technology,* 111, 2021, 106518.

[43] SALOME, Available online: https://www.salome-platform.org.
[44] Mastrone, M. N., Hartono, E. A., Chernoray, V. and Concli, F., Oil distribution and churning losses of gearboxes: Experimental and numerical analysis, *Tribology International,* 151, 2020, 106496.
[45] Mastrone, M. N. and Concli, F., Power Losses of Spiral Bevel Gears: An Analysis Based on Computational Fluid Dynamics, *Frontiers in Mechanical Engineering,* 7, 2021, 40.

ORCID iD

Marco Nicola Mastrone https://orcid.org/0000-0001-5228-6467
Franco Concli https://orcid.org/0000-0002-1237-5542

How to cite this article: Mastrone M.N., Concli F. Numerical Modeling of Fluid's Aeration: Analysis of the Power Losses and Lubricant Distribution in Gearboxes, *J. Appl. Comput. Mech.*, 9(1), 2023, 83–94. https://doi.org/10.22055/jacm.2022.40666.3625